Reaction Chemistry & Engineering

Catalytic co-pyrolysis of LDPE and PET with HZSM-5, H-Beta, and HY: Experiments and kinetic modelling

Journal:	*Reaction Chemistry & Engineering*
Manuscript ID	RE-ART-04-2022-000144.R1
Article Type:	Paper
Date Submitted by the Author:	28-May-2022
Complete List of Authors:	Okonsky, Sean; Penn State University Park Jonnalagedda, Varaha Jayarama Krishna; Penn State University Park Toraman, Hilal Ezgi; Penn State University Park

ARTICLE

Catalytic co-pyrolysis of LDPE and PET with HZSM-5, H-Beta, and HY: Experiments and kinetic modelling

Received 00th January 20xx,
Accepted 00th January 20xx

DOI: 10.1039/x0xx00000x

Sean Timothy Okonsky,[a] J.V. Jayarama Krishna [b] and Hilal Ezgi Toraman [*a,b,c]

In this study, the catalytic pyrolysis of low-density polyethylene (LDPE), polyethylene terephthalate (PET) and their mixture (1:1 wt./wt.) with three zeolite catalysts (HZSM-5, H-Beta, HY) was investigated using a thermogravimetric analyzer (TGA) and a Pyroprobe® micro-reactor coupled to a gas chromatograph mass spectrometer (Py-GC/MS). The TGA results demonstrated that during pyrolysis at 10 °C/min, on average, zeolite catalysts decreased the maximum decomposition temperature by 149 °C for LDPE while only decreasing by 8 °C for PET. The derivative thermogravimetric (DTG) curve evidenced interactions when the two polymers were catalytically co-pyrolyzed for all the three catalysts. A lumped n^{th} order reaction scheme was able to accurately model both non-catalytic and catalytic pyrolysis and co-pyrolysis by using least squares fitting approach for determining the kinetic parameters. The kinetic model was able to model well the interaction effects observed during catalytic co-pyrolysis of LDPE and PET with HZSM-5, H-Beta, and HY ($Fit\%_{Wt\%}$ > 96%, $Fit\%_{DTG}$ > 94%). Py-GC/MS experiments for the catalytic fast pyrolysis of LDPE revealed HZSM-5 resulted in the highest selectivity to aromatic hydrocarbons (31.6%) and HY resulted in the highest selectivity to gasoline range C_5-C_{10} paraffins and olefins (40.9%). Catalytic fast pyrolysis of PET showed high selectivity to benzene for all catalysts (> 43%) and that HZSM-5 resulted in the highest selectivity to polyaromatic hydrocarbons (24.7%). The catalytic fast co-pyrolysis of LDPE and PET revealed interaction effects for all the three catalysts evidenced by a positive synergy% for alkylated benzenes (3-142%) and polyaromatics (105-187%) with a concomitant negative synergy% for benzene (24-36%) and C_5-C_{10} paraffins and olefins (27-53%).

1. Introduction

Since their inception in the early 1900s, plastics have become an essential resource for our global society being used in packaging, construction materials, textiles, vehicles, and electronics. In 2015, over 400 million metric tons (MMT) of plastics were produced, and this number is expected to continually rise each year.[1] The disposal of plastics is a global issue as it has been shown that plastics are responsible for 60-80% of total marine debris which have led to the formation of the great pacific garbage patch with an estimated surface area of 1.6 million square kilometers.[2] In addition to harming our environment, waste plastics are estimated to contribute to an economic loss of 80-120 billion USD annually.[3] A review of life cycle analyses has concluded that recycling plastics saves about 1.5-2 tons of carbon dioxide per ton of plastic recycled, when compared to the alternatives of landfill and incineration with energy recovery.[4] Mechanical recycling is a process in which plastic waste is sorted, shredded, washed, and extruded into plastic pellets. During the melt processing of the plastic, heating and mechanical shearing of the polymer results in a decrease in its average molecular weight, thus resulting in a loss in quality.[5] This compromised performance causes 47% of recycled polyethylene terephthalate (rPET) to be converted into fibers which can be used for clothing and carpet, while only 21% is used for food and beverage bottles.[6] While clothing made with rPET has eco-friendly appeal, it is estimated that the washing of these synthetic garments leads to an accumulation of half a million tons of microplastics in the ocean per year.[7] In 2015, three of the main polyolefin polymers viz., low-density polyethylene (LDPE), high-density polyethylene (HDPE), and polypropylene (PP) alone contributed to 19.7 MMT of waste per year in the USA of which only 8.3% was recycled.[1] Multilayer packaging often contains a blend of polymers including PET and polyolefins, and requires complex delamination procedures for its recycling, thus markedly reducing its overall recycling rate.[8,9]

Pyrolysis is a process of thermal degradation of feedstocks in inert ambience. It is an attractive alternative to mechanical recycling for the processing of plastic waste, as it can process both single streams of plastics in addition to mixtures of plastics at large volumes. Polyolefin plastics such as PP, HDPE, and LDPE are attractive feedstocks for pyrolysis due to their high hydrogen to carbon ratio.[10,11] The non-catalytic degradation of polyolefins occurs via random radical scission mechanism and can produce high molecular weight waxes, C_5-C_{20} range liquid alkanes and alkenes, and light gases such as ethylene and

[a] Department of Chemical Engineering, Pennsylvania State University, University Park, PA- 16801, USA
[b] Department of Energy and Mineral Engineering, Pennsylvania State University, University Park, PA- 16801, USA
[c] Institutes of Energy and the Environment, Pennsylvania State University, University Park, PA- 16801, USA, E-mail: hzt5148@psu.edu

† Footnotes relating to the title and/or authors should appear here.
Electronic Supplementary Information (ESI) available: [details of any supplementary information available should be included here]. See DOI: 10.1039/x0xx00000x

propylene.[11,12] Depending on the pyrolysis temperature used, wide ranges of yields for gas (11-71 wt%), oil (25-44 wt%), and wax (4-45 wt%) can be obtained.[13] The non-catalytic pyrolysis of PET results in low oil yields (2-24 wt%) and high yields of gas (37-49 wt%) and solid products (35-49 wt%).[14,15] The non-catalytic pyrolysis of PET occurs via a 6-membered ring transition state which leads to the production of carbon dioxide, carbon monoxide, and solid waxy oxygenates such as terephthalic acid and benzoic acid.[16]

The catalytic pyrolysis of polyolefins can help to tailor product distribution to increase the production of light olefins, gasoline, or diesel range hydrocarbons depending on the type of catalyst used. Acid catalyst zeolites have been widely used for polyolefins and act by promoting the carbocationic cracking of pyrolysis volatiles and subsequent reactions of isomerization, oligomerization-cracking and hydrogen transfer.[11] For HZSM-5 with varying Si:Al ratios leading to varying acidity, it is known that higher total acidity increases the capacity to crack C_5-C_{11} non-aromatic fractions and to condensate C_2-C_4 olefins leading to increased production of aromatic compounds.[17] When different zeolite structures with varying pore sizes are used for polyolefin pyrolysis, it well known that larger pore size leads to heavier carbon products, higher paraffin/olefin ratio, and higher coke formation.[18–20] Zeolites have shown the ability to aid in the decarboxylation of benzoic acid and terephthalic acid during PET pyrolysis, resulting in high yields of benzene.[21,22] In comparison with CaO catalyst, HZSM-5 zeolite catalyst was shown to produce a higher amount of benzene derivatives, indenes and naphthalenes during the catalytic pyrolysis of PET waste carpet.[23]

Investigation of the co-pyrolysis of PET with polyolefins is valuable as the simultaneous pyrolysis of these mixed polymers would allow for the following: (i) the ability to process large volumes of mixed plastics in pyrolysis plants without the need of prior separation, (ii) providing an alternative to mechanical recycling for PET waste, and (iii) enhancing the ability to process inherently mixed plastics such as multilayer packaging containing both polyolefins and PET. It has been shown that during co-pyrolysis, the presence of PET helps to decrease the degradation temperature for HDPE.[24] The pyrolysis of 50%/50% PE/PET mixtures with metal loaded zeolite catalysts have been shown to produce oil yields as high as 52.9%.[25,26] When conducting catalytic co-pyrolysis of PE and PET with HZSM-5 catalyst in a micro-reactor, an interaction effect which showed an increase in benzene and alkylated benzenes and a decrease in solid residue, C_1-C_5 alkanes/alkenes, and CO_2 was observed.[21]

Thermogravimetric analysis (TGA) is a powerful tool which allows the study of degradation kinetics for various feedstocks by obtaining the mass loss data as a function of time and temperature. The kinetic triplet viz., activation energy (E_a), pre-exponential factor (A), and reaction order (n) can be obtained from TGA data using various approaches reported in the literature. Isoconversional approaches such as the Flynn-Wall-Ozawa (FWO) method and the Coats-Redfern (CR) method use TGA data ran at various heating rates to determine the activation energy (E_a) for various values of conversion, and will often assume a first order reaction model to estimate the pre-exponential factor.[27,28] Few authors have also used least squares fitting method and lumped reaction schemes to derive kinetic parameters which can model the polymer decomposition for the catalytic pyrolysis of plastic waste as well as for the co-pyrolysis of biomass with plastics.[29,30] An incorporation of isoconversional approach with least squares fitting technique has been used to model the non-catalytic pyrolysis of biomass,[31,32] but to the best of our knowledge an incorporation of the two has not been used for modeling the catalytic co-pyrolysis of mixed plastic waste.

While most thermal and catalytic studies focus on individual polymers,[13–15,17,22] the interaction effects between polymers are rarely studied in a systematic way.[33,34] To the best of our knowledge, the catalytic co-pyrolysis of LDPE and PET for multiple zeolite frameworks has not been studied via either TGA or analytical pyrolysis-gas chromatography/mass spectrometry (Py-GC/MS). The objectives of this study are three-fold. Firstly, to obtain kinetic parameters for the non-catalytic and catalytic degradation of LDPE, PET, and their mixtures in equal proportions using least squares fitting technique. Secondly, to study the composition of pyrolysis vapors from LDPE and PET in the presence of three catalysts viz., HZSM-5, H-Beta, and HY. Thirdly, to analyze the synergistic effects observed during the catalytic co-pyrolysis of LDPE and PET.

2. Experimental

2.1 Materials

Low-density polyethylene (LDPE) and polyethylene terephthalate (PET) powders were supplied from Goodfellow Corporation (Coraopolis, PA, United States). Item numbers were ET316031 and ES306031 for LDPE and PET, respectively. Particle size of both polymer powders was less than 300 µm. LDPE was specified by the vendor to be additive free, and PET contained 1 ppm acetaldehyde. ZSM-5 (CBV2314), zeolite Beta (CP814C*), and zeolite Y (CBV600) catalysts were supplied from Zeolyst international. All catalysts were sieved to a particle size of 210 µm < 250 µm prior to calcination. Catalysts were calcinated using a 5 °C/min ramp to 550 °C then held at 550 °C for 5 h in a tube furnace with air flow. Post calcination, zeolites were stored in a glove box until they were used for experiments.

2.2 Catalyst Characterization

2.2.1 N_2 Physisorption

A Micromeritics ASAP 2020 surface analysis instrument was used to compute the BET surface area, the external surface area, and the micropore volume of each catalyst. A catalyst mass of 0.12 g was loaded in the analysis tubes and heated to 200 °C for a period of 2 h to desorb any adsorbed water prior to analysis. Analysis was conducted at 77 K and partial pressure (P/P_0) values from 0.0025 to 0.994 were recorded (Figure S1). 10 P/P_0 values in the range of 0.05-0.3 were used to compute the BET surface area and 8 P/P_0 values in the range of 0.05-0.3

were used to compute the micropore volume and the external surface area via the t-plot method.[35]

2.2.2 NH_3 Temperature Programmed Desorption (NH_3-TPD)

NH_3-TPD experiments were ran using a Micromeritics Autochem II 2920 Chemisorption analyzer for comparing total acidity of the catalysts,[36] as well as for determining relative acid strength. A catalyst mass of 0.12 g was weighed and added to the instrument. Helium flowrate of 50 mL/min was passed over the catalyst while temperature was raised to 300 °C and held for 2 h to remove any moisture. The catalyst was then cooled to 50 °C. Once cooled, the flow was switched to 50 mL/min of 15% NH_3/He for 1 h to saturate the catalyst with ammonia. The flow was then switched back to 50 mL/min of helium at 50°C for 1 h to remove any physiosorbed ammonia. The temperature was then raised at a ramp of 10 °C/min to 500 °C and held at 500 °C for 1 h to desorb chemisorbed NH_3 while the NH_3 signal was recorded with a thermal conductivity detector (Figure S2). The relative acid strength of catalytic sites was determined using peak deconvolution. The NH_3 desorption in the temperature regions of 120-200 °C, 200-350 °C, and 350-450°C correspond to weak, medium, and strong acid sites respectively (Figure S3, Table S5).[37]

2.2.3 Pyridine TPD

Pyridine TPD was used as a method to quantify the acidity of the zeolites as has been done by Osman et al.[38] Pyridine was first dosed onto catalysts using a horizontal tube furnace. The calcinated catalyst of 100 mg was placed in an alumina crucible in the tube furnace and then under nitrogen flow, the furnace was raised to 207 °C for 30 min. The nitrogen flow was then redirected to first go through a glass saturator filled with pyridine (Sigma-Aldrich, 99%) before flowing into the tube furnace. Nitrogen was kept flowing through pyridine for 2 h at 207 °C before switching back to pure nitrogen flow for 30 min at 207 °C to remove any physiosorbed pyridine molecules. 12 mg of pyridine loaded catalyst was added to a TGA crucible and analyzed to determine the pyridine loading. The TGA furnace was first brought to 200 °C to remove any adsorbed water from the pyridine loaded zeolite. Then, the temperature was increased to 800 °C at a ramp rate of 5 °C/min and held at 800 °C for 1 h, and the weight change between 200°C and 800°C, represented as $m_{pyr\_C,200°C} - m_{pyr\_C,800°C}$, was defined as the weight of adsorbed pyridine.

Pyridine loading was then calculated using the molar mass of pyridine in Eq. (1): $m_{pyr\_C,200°C} - m_{pyr\_C,800°C}$ is the weight change of pyridine loaded catalyst measured via TGA between 200 °C and 800 °C (mg). $m_{pyr\_C,800°C}$ is equal to the mass of catalyst post pyridine adsorption (mg).

$$\frac{mmol\ Pyr}{g_{cat}} = \frac{\left(m_{pyr\_C,200°C} - m_{pyr\_C,800°C}\right) \times \frac{79.1mmol}{mg}}{m_{pyr\_C,800°C} \times \frac{1g}{1000mg}} \quad (1)$$

2.2.4 Attenuated Total Reflectance Fourier Transform Infrared (ATR-FTIR) Spectroscopy

A Bruker Vertex V70 FTIR spectrometer was used with a Harrick DiaMax ATR accessory to determine the Brønsted : Lewis acid ratio for pyridine loaded zeolites obtained from the method described in Section 2.2.3. A total of 400 scans were taken at room temperature with six wave number resolution and the spectra were detected with a liquid nitrogen cooled mercury cadmium telluride (LN-MCT) detector (Figure S4). The areas under peaks at 1545 cm^{-1} and 1455 cm^{-1} and extinction coefficients of 1.67 and 2.22 were used to determine the relative amount of Brønsted and Lewis acid sites respectively.[39]

2.2.5 Aluminum Nuclear Magnetic Resonance (^{27}Al NMR) Spectroscopy

Solid-state magic angle spinning (MAS) NMR measurements were performed on a Bruker Avance-III-HD console in conjunction with a wide bore Magnex magnet. Zeolites were removed from the glovebox and then outside of the glovebox were loaded into a 4 mm MAS rotor. The spectrometer frequency was 130.25 MHz. The samples were spun at a frequency of 12 KHz, and 10,240 scans were recorded (Figure S5-S7). Calibrations were performed for ^{27}Al with $AlCl_3(H_2O)_6$ as a reference at 0 ppm. The areas under peaks at 60 ppm, 30 ppm, and 0 ppm were used to quantify the amount of AlO_4 framework aluminate species (FAl), AlO_5, and AlO_6 extra-framework species (EFAl), respectively to determine the percentage of framework aluminum.

2.3 Thermogravimetric Analysis (TGA)

A TA instruments Q600 SDT DSC-TGA thermal analyzer was used to conduct TGA experiments to determine the degradation profile of polymers with and without catalyst. A heating rate of 10 °C/min was used with a helium flowrate of 100 mL/min (Praxair 99.999%). The mass of the polymer feedstock was 7.5 mg, and a catalyst to feedstock ratio of 1:1 wt./wt. was used resulting in a total mass of 15 mg for catalytic experiments. For catalytic co-pyrolysis experiments, an LDPE:PET feedstock ratio of 1:1 wt./wt. was used. Polymer and catalysts were well mixed in glass vials for a period of 5 min prior to being added to the TGA crucible. Water was desorbed from the polymer/catalyst mixture by holding the mixture at a temperature of 80 °C, below the melting point of both polymers, for 2 h in the TGA furnace. Each experiment was performed a minimum of two times and figures shown represent an average of repeated runs. Standard deviation for TGA curves can be seen in Figure S8.

Polymer wt.% for a given time, t=*i*, was calculated using Eq. (2)-(4). Due to the hygroscopic nature of the zeolite catalysts, some water is desorbed from the catalysts during TGA experiments. To avoid misinterpreting this water desorption for degradation of polymer during catalytic pyrolysis, additional TGA experiments were conducted with 7.5 mg of only catalyst to determine the weight fraction curve for water adsorbed catalyst described in Eq. (2). This was then subtracted from the catalytic pyrolysis curve, taking into account the catalyst to feedstock ratio (CF) (Eq. (3)), to determine the mass of polymer

at a given time t=*i* during catalytic pyrolysis. This was divided by the initial mass of polymer, which resulted in a TGA curve representative of polymer weight% (Eq. (4)). The derivative weight% (DTG) curve was then calculated using Eq. (5).

$$w_{cat,t=i} = \frac{m_{cat,t=i}}{m_{cat,t=0}} \quad (2)$$

$$CF = \frac{wt_{cat,mix}}{wt_{pol,mix}} \quad (3)$$

$$Pol\ Wt\%_{t=i} = \frac{m_{CP,t=i} \times \left[1 - \left(\frac{CF}{1+CF}\right) \times w_{cat,t=i}\right]}{m_{CP,t=0} \times \left[1 - \left(\frac{CF}{1+CF}\right)\right]} \times 100\% \quad (4)$$

$$\frac{dWt\%}{dT}_{t=i} = \frac{Pol\ Wt\%_i - Pol\ Wt\%_{i-1}}{T_{t=i} - T_{t=i-1}} \quad (5)$$

where $m_{cat,t=i}$ is the recorded weight from TGA of the catalyst-only run at a given time *i* (mg), $w_{cat,t=i}$ is the measured weight fraction for the catalyst-only run at a given time *i*, $wt_{cat,mix}$ is the weight of catalyst added to the vial which was used for pre-mixing procedure (mg), $wt_{pol,mix}$ is the weight of polymer added to the vial which was used for pre-mixing procedure (mg), $m_{CP,t=i}$ is the recorded weight from TGA of the catalytic pyrolysis run at a given time *i* (mg), and $T_{t=i}$ is the temperature for the TGA at a given time point *i* (°C).

2.4 Micro-pyrolysis Gas Chromatography Mass Spectrometry (Py-GC/MS)

A CDS Pyroprobe® 6200 micro-reactor was used to pyrolyze the polymer samples. The micro-reactor was interfaced with a Thermo Scientific ISQ LT Single Quadrupole Gas Chromatograph/Mass Spectrometer (GC/MS) for separation and identification of compounds. Polymer/catalyst samples were loaded into drop in sample chamber (DISC) quartz tubes which had an inner dimeter of 1.9 mm and a total length of 38 mm. For all the experiments, a catalyst to feedstock ratio of 10:1 was used. For catalytic co-pyrolysis experiments, an LDPE:PET feedstock ratio of 1:1 was used. Polymer and catalyst were pre-mixed in a glass vial prior to sample loading. 2.2 ± 0.1 mg of the plastic/catalyst mixture was added to the quartz tube resulting in a plastic feedstock weight of 0.2 mg. The sample loaded quartz tubes were then placed in an autosampler which would then drop each tube into the platinum filament surrounded reaction chamber for analysis. Once the tube was dropped into the chamber, the platinum filament would heat at a heating rate of 20,000 °C/s to the pyrolysis temperature, which for these experiments was set to be 500 °C, for a period of 120 s. Krishna et al. have showed using COMSOL software that for a coil heating rate of 20,000 °C/s, the average heating rate of polymer feedstocks in the Pyroprobe® reactor is in the range of 125-150 °C/s.[40] The pyrolysis vapors were sent to the GC for online analysis using a carrier gas of helium (Praxair 99.999%) with a constant flow rate of 126.5 mL/min. Split/splitless injector was used for GC/MS analysis and its temperature was set at 300 °C. The GC inlet split ratio was set to 80 and a column flow rate of 1.5 mL/min was used. A 60-meter Thermo TG-1MS column with 0.25 mm inner diameter, and 0.25 µm film thickness was used. The GC oven was initially held at 35 °C for 3 min, ramped to 280 °C at 6 °C/min, and held at 280 °C for 5 min. The mass spectrometer m/z scan range was 29-550. Utilizing Xcalibur software and NIST MS Search v.2.3 pyrolysis products were identified and semi-quantified through determining peak area%, which corresponds to the selectivity of pyrolysis vapors.

Each experimental condition was repeated three times, and an average and standard deviation of area% for products were reported. The calculations for additive area%, the area% expected to be observed for a compound or compound class "X" during co-pyrolysis if no interaction effects were present, can be found in Section S1 of Supplementary Information. Synergy% is calculated using Eq. (6) which involves the additive area%. A positive synergy% indicates a positive interaction effect in which more of the compound was formed during co-pyrolysis than would be expected. A negative synergy% indicates a negative interaction effect in which less of the compound was formed during co-pyrolysis than would be expected.

$$Synergy\% = \frac{Experimental\ area\% - Addtive\ area\%}{Addtive\ area\%} \times 100 \quad (6)$$

3. Kinetic Analysis

In previous papers, Marcilla et al. proposed and applied kinetic models to describe the catalytic pyrolysis of LDPE with HZSM-5 and H-Beta catalysts using a lumped model fitting approach.[29] For this work, the approach applied by Marcilla et al. for the catalytic pyrolysis of LDPE over HZSM-5 has been extended to model the catalytic pyrolysis of PET and the catalytic co-pyrolysis of LDPE and PET using the reaction scheme (R1)-(R4) as shown below.

$$LDPE \xrightarrow{k_{NC,L}} G1 \quad (R1)$$

$$LDPE + aC \xrightarrow{k_{C,L1}} (1+a)LDPEC \xrightarrow{k_{C,L2}} \alpha G2 + (1-\alpha)(Coke + aC_{coked}) + \alpha aC \quad (R2)$$

$$PET \xrightarrow{k_{NC,P}} \gamma G3 + (1-\gamma)Char \quad (R3)$$

$$PET + bC \xrightarrow{k_{C,P1}} (1+b)PETC \xrightarrow{k_{C,P2}} \beta G4 + (1-\beta)(Coke + bC_{coked}) + b\beta C \quad (R4)$$

The model above assumes that both LDPE and PET can decompose either via non-catalytic degradation (R1 and R3) or catalytic degradation (R2 and R4) during catalytic pyrolysis. The subscripts NC and C refer to non-catalytic and catalytic reaction pathways, respectively. LDPE and PET are the two polymers, C represents active catalyst, LDPEC and PETC are intermediates formed during catalytic degradation, G1-G4 represent the volatiles formed through their respective pathways, Char is solid residual formed during the non-catalytic degradation of PET, Coke is solid residual formed during the catalytic degradation of LDPE and PET, and C_{coked} is catalyst which has been coked and can no longer catalytically degrade the polymers. The stoichiometric coefficients a and b represent the

grams of catalyst per gram of LDPE and PET necessary to obtain the complexes LDPEC and PETC, respectively. Solid residual stoichiometric coefficients (α, γ, β) have been added to the kinetic model for the formation of Char and Coke, as has been done by Marcilla et al. when modeling the deactivation of HZSM-5 during the catalytic pyrolysis of LDPE.[41] The term α corresponds to the mass fraction of LDPE in the LDPEC complex which is converted into volatile product "G2" during catalytic degradation of LDPE (R2). The term $(1-\alpha)$ represents the mass fraction of LDPE in the LDPEC complex which is converted to Coke. The same applies for β for the catalytic degradation of PET (R4). The term γ corresponds to the mass fraction of PET which is converted to volatiles during non-catalytic pyrolysis (R3) and $(1-\gamma)$ represents the mass fraction of PET converted to char.

This model assumes a single step catalytic degradation of both LDPE and PET. It can be used to reproduce the non-catalytic and catalytic decomposition of LDPE and PET both when pyrolyzed separately (single-stream) and together (co-pyrolysis). Assuming nth order reaction kinetics, the kinetic differential equations to model the pyrolysis become:

$$\frac{d[LDPE]}{dt} = -k_{NC,L}[LDPE]^{n_{NC,L}} - k_{C,L1}[LDPE]^{n_{C,L1\_L}}[C]^{n_{C,L1\_C}} \quad (7)$$

$$\frac{d[LDPEC]}{dt} = (1+a)k_{C,L1}[LDPE]^{n_{C,L1\_L}}[C]^{n_{C,L1\_C}} - (1+a)k_{C,L2}[LDPEC]^{n_{C,L2}} \quad (8)$$

$$\frac{d[PET]}{dt} = -k_{NC,P}[PET]^{n_{NC,P}} - k_{C,P1}[PET]^{n_{C,P1\_P}}[C]^{n_{C,P1\_C}} \quad (9)$$

$$\frac{d[PETC]}{dt} = (1+b)k_{C,P1}[PET]^{n_{C,P1\_P}}[C]^{n_{C,P1\_C}} - (1+b)k_{C,P2}[PETC]^{n_{C,P2}} \quad (10)$$

$$\frac{d[C]}{dt} = -ak_{C,L1}[LDPE]^{n_{C,L1_L}}[C]^{n_{C,L1C}} + a\alpha k_{C,L2}[LDPEC]^{n_{C,L2}} - bk_{C,P1}[PET]^{n_{C,P1\_P}}[C]^{n_{C,P1\_C}} + b\beta k_{C,P2}[PETC]^{n_{C,P2}} \quad (11)$$

$$\frac{d[Coke]}{dt} = (1-\alpha)k_{C,L2}[LDPEC]^{n_{C,L2}} + (1-\beta)k_{C,P2}[PETC]^{n_{C,P2}} \quad (12)$$

$$\frac{d[C_{coked}]}{dt} = a(1-\alpha)k_{C,L2}[LDPEC]^{n_{C,L2}} + b(1-\beta)k_{C,P2}[PETC]^{n_{C,P2}} \quad (13)$$

$$\frac{d[Char]}{dt} = (1-\gamma)k_{NC,P}[PET]^{n_{NC,P}} \quad (14)$$

$$\frac{d[G1]}{dt} = k_{NC,L}[LDPE]^{n_{NC,L}} \quad (15)$$

$$\frac{d[G2]}{dt} = \alpha k_{C,L2}[LDPEC]^{n_{C,L2}} \quad (16)$$

$$\frac{d[G3]}{dt} = \gamma k_{NC,P}[PET]^{n_{NC,P}} \quad (17)$$

$$\frac{d[G4]}{dt} = \beta k_{C,P2}[PETC]^{n_{C,P2}} \quad (18)$$

Species in bracketed terms are representative of their mass fraction. $n_{cat,pol,k}$ is the reaction order where "cat" can be either NC or C depending on whether the reaction is non-catalytic or catalytic, "pol" can be either L or P for LDPE and PET respectively, and "k" is either 1_pol, 1_C, or 2 for [pol], [C], and [polC] respectively for reactions R2 and R4. The rate constants $k_{cat,pol,i}$ are expressed by the Arrhenius law for reaction *i* for a given catalyst and polymer:

$$k_{cat,pol,i} = A_{cat,pol,i} \times \exp\left(-\frac{E_{cat,pol,i}}{RT}\right) \quad (19)$$

where *A* is the pre-exponential factor (s^{-1}), *E* is the apparent activation energy (kJ/mol), *R* is the universal gas constant (8.314E-3kJ/mol*K), and *T* is the absolute temperature (K). A mass balance on the polymeric species leads to:

$$[LDPE] + [PET] + \frac{1}{1+a}[LDPEC] + \frac{1}{1+b}[PETC] + [Char] + [Coke] + [G1] + [G2] + [G3] + [G4] = 1 \quad (20)$$

The mass balance on the catalyst species leads to:

$$[C] + \frac{a}{1+a}[LDPEC] + \frac{b}{1+b}[PETC] + [C_{coked}] = CF \quad (21)$$

Where the catalyst : feedstock ratio, CF, is equal to 1 for catalytic experiments and 0 for non-catalytic experiments for this paper. An initial boundary condition of [LDPE] = 1 and [PET] = 0, [PET] = 1 and [LDPE] = 0, and [LDPE] = 0.5 and [PET] = 0.5 at t = 0 is used for the single-stream pyrolysis of LDPE, PET, and the 1:1 co-pyrolysis of LDPE and PET, respectively. For catalytic pyrolysis modeling, [C] = 1 at t = 0, and for non-catalytic pyrolysis modeling, [C] = 0 at t = 0. All other species in the kinetic model are set equal to 0 at t = 0. Euler's method was utilized to integrate the kinetic equations, solving for the mass fraction of species for a given point *i* in the temperature ramp program, ultimately solving for a model polymer weight% and DTG curve where:

$$Pol\ wt\%_{mod,i} = \left[[LDPE]_i + [PET]_i + \frac{1}{1+a}[LDPEC]_i + \frac{1}{1+b}[PETC]_i + [Char]_i + [Coke]_i\right] \times 100\% \quad (22)$$

$$dWt\%/dT_{mod,i} = \frac{Pol\ wt\%_{mod,i} - Pol\ wt\%_{mod,i-1}}{T_i - T_{i-1}} \quad (23)$$

An objective function was used in order to solve for kinetic parameters which would give a model close in nature to the experimental results:

$$Objective = \sum_{F=1}^{3}\sum_{i=1}^{n_d}\left\{\left[\left(\text{Pol wt\%}_{i,F}\right)_{exp} - \left(\text{Pol wt\%}_{i,F}\right)_{model}\right]^2 + 100\left[\left(\text{dWt\%/dT}_{i,F}\right)_{exp} - \left(\text{dWt\%/dT}_{i,F}\right)_{model}\right]^2\right\} \quad (24)$$

where F ranging from 1 to 3 represents the three feedstock combinations used in this study (LDPE, PET, LDPE+PET) and *i* ranging from 1 to n_d represents the number of data points obtained experimentally. The Solver tool in Microsoft Excel was used to vary kinetic parameters to minimize the objective function for both non-catalytic and catalytic pyrolysis with HZSM-5, H-Beta, and HY. Kinetic parameters for the non-

catalytic pyrolysis of LDPE and PET were first solved using Flynn-Wall-Ozawa (FWO) isoconversional approach as outlined in Section S2 of Supplementary Information. The activation energy and pre-exponential factor obtained from FWO approach were used as initial guesses for the n^{th} order non-catalytic pyrolysis parameters of $E_{NC,P}$, $E_{NC,L}$, $A_{NC,P}$, and $A_{NC,L}$.[32] Once the non-catalytic pyrolysis parameters were solved for, they were utilized for modeling the catalytic pyrolysis experiments. When solving for the catalytic parameters, the non-catalytic pyrolysis parameters were included but not allowed to vary. To judge the goodness of fit for the model curves to the experimental curves, the following equations for Fit% were used as has been done in other kinetic modeling work.[42] In these equations, S is the objective function for DTG data, S^1 is the objective function for polymer wt% data, n_d is the number of data points recorded for a TGA run, and $\left(\frac{dWt\%}{dT}\right)_{max}$ is the maximum DTG value for the experimental data.

$$Fit\%_{DTG} = \left(1 - \frac{\sqrt{\frac{S}{n_d}}}{\left(\frac{dWt\%}{dT}\right)_{max}}\right)100\% \quad (25)$$

$$Fit\%_{Wt\%} = \left(100\% - \sqrt{\frac{S^1}{n_d}}\right) \quad (26)$$

where:

$$S = \sum_{i=1}^{n_d}[(dWt\%/dT_i)_{exp} - (dWt\%/dT_i)_{model}]^2 \quad (27)$$

$$S^1 = \sum_{i=1}^{n_d}[(Pol\ wt\%_i)_{exp} - (Pol\ wt\%_i)_{model}]^2 \quad (28)$$

4. Results and Discussion

4.1 Catalyst Characterization

The results from catalyst characterization measurements are shown in Table 1. It is seen that the trend of surface area is consistent with that reported by Zeolyst. Micropore volume increases for the catalysts as the pore size of the zeolite framework increases. Calculated pyridine loading shows that the total acidity of HZSM-5 > H-Beta > HY. This is confirmed by the trend observed during NH_3 TPD experiments (Figure S2). Typically, it is thought that lower Si:Al ratio leads to higher acidity,[19] however HY with the lowest Si:Al ratio in our case shows the lowest acidity. This is due to the large percentage of non-framework aluminum in the HY catalyst compared with HZSM-5 and H-Beta. CBV600 is produced by the steaming of CBV300, and framework aluminum, which is responsible for Brønsted acid sites, is displaced in the process.[43,44] Extra framework aluminum (EFAl) species are often associated with Lewis acid sites, and this substantiates the fact that HY with the highest EFAl content has the lowest Brønsted : Lewis acid ratio among the three catalysts.[44] It is seen that HZSM-5 has the highest acid strength of the three catalysts, evidenced by its highest proportion of medium and strong acid sites determined from NH_3-TPD (Figure S3 and Table S5).

Table 1. Physico-chemical properties measured for the three zeolites used in this study

Zeolite type	HZSM-5 (CBV2314)	H-Beta (CP814C*)	HY (CBV600)
SiO_2/Al_2O_3 Mole Ratio	23	38	5.2
Pore diameter (Å)	5.3×5.6 5.1×5.8	5.5×5.5 7.6×6.4	7.4×7.4
BET surface area (m^2/g_{cat})	317	551	459
External surface area (m^2/g_{cat})	100	182	64
Micropore volume (cm^3/g_{cat})	0.116	0.194	0.207
Weak : medium : strong acid ratio	1:1.7:1.8	1:0.5:1	1:0.9:1.1
Pyridine loading (mmol Pyr/g_{cat})	1.346	0.832	0.735
Brønsted : Lewis acid ratio	80.5:1	5.3:1	1.1:1
% Framework aluminium	76.9	74.5	35.5

4.2 Thermogravimetric Analysis

4.2.1 Effect of catalyst on LDPE pyrolysis

It can be observed from Figure 1 that for the pyrolysis of LDPE at 10 °C/min, the effect of catalyst on the degradation temperature is substantial. The maximum degradation temperature (T_{max}) for LDPE non-catalytic pyrolysis and LDPE pyrolysis with HZSM-5, H-Beta, and HY catalyst was found to be 472.4 °C, 314.7 °C, 312.2 °C, and 344.5 °C, respectively. It is known that for the catalytic pyrolysis of LPDE with zeolite catalysts, that higher external surface area helps to decrease T_{max} and increase conversion during pyrolysis.[29,45] It has been proposed that the external surface helps to pre-crack polymer macromolecules, forming oligomers, which are then subsequently cracked in the internal structure of the zeolite.[29] In addition to external surface area, higher acidity is also known the decrease pyrolysis decomposition temperature.[46] This explains why HZSM-5, which had the highest acidity and moderate external surface area, and H-Beta, which had moderate acidity and the highest external surface area, both resulted in similar T_{max} values. HY, which had the lowest acidity and the lowest external surface area, had the highest T_{max} value. In addition to having the highest T_{max} value, HY resulted in a shorter wider peak in its DTG curve, indicating that LDPE was degrading over a larger temperature range than for HZSM-5 and H-Beta. A similar trend was also observed by others for the catalytic pyrolysis of LDPE with HY in comparison with H-Beta, H-Mordenite, and H-Ferrierite.[46] It is observed that LDPE/HZSM-5 results in a lower amount of residual polymer left in the TGA crucible (0.6%) than for LDPE/H-Beta (6.2%) and LDPE/HY (9.7%). It is known that H-Beta and HY both undergo significantly higher deactivation during the catalytic pyrolysis of LDPE when compared to HZSM-5.[20,47] This trend is also observed in our study as the solid residual, resemblant of catalytic coke, is higher for H-Beta and HY. The conversion for LDPE/H-Beta (93.8%) is similar to that reported by Pyra et al. (97.5%) where the

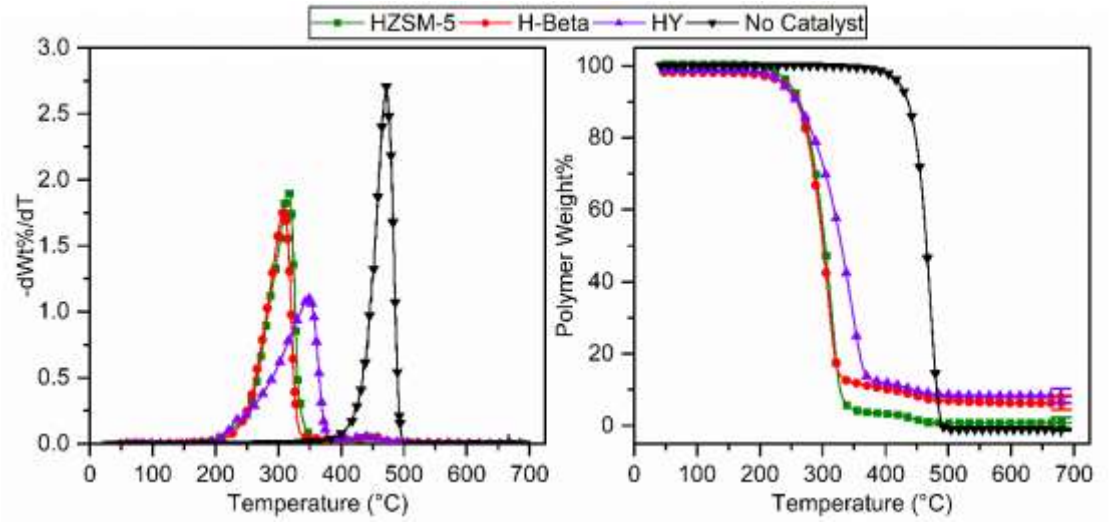

Figure 1. Derivative thermogravimetric (DTG) and polymer weight percent curves for LDPE pyrolysis at 10 °C/min in the presence or absence of catalyst at a 1:1 catalyst to feedstock ratio.

authors used a 1:3 catalyst to feedstock ratio and 5 °C/min heating rate during thermogravimetric analysis.[48]

4.2.2 Effect of catalyst on PET pyrolysis

In Figure 2, it can be observed that the addition of catalyst does not decrease T_{max} as much for PET as it does for LDPE. These results are in line with that observed in the literature for zeolite catalysts where the decrease in T_{max} is more pronounced for polyolefins than for PET.[21,49] T_{max} for PET non-catalytic pyrolysis and PET pyrolysis with HZSM-5, H-Beta, and HY catalyst was observed to be 432.2 °C, 432.2 °C, 389.8 °C, and 426.1 °C, respectively. This low decrease in T_{max} leads to an overlap of the catalytic DTG curves with the non-catalytic DTG curve. The area under the catalytic DTG curve which exists at lower temperatures than the non-catalytic DTG curve can be interpreted as a measure of the catalytic volatilization of PET. The area under the catalytic DTG curve which overlaps the non-catalytic DTG curve may be interpreted as a measure for the non-catalytic volatilization of PET which occurs even in the presence of catalyst.

It can be seen in Figure 2 that H-Beta results in the highest amount of catalytic volatilization. The catalytic pyrolysis of PET shows to have a shoulder to its main degradation peak. The shoulder for PET/H-Beta (421 °C) lies in the regime of non-catalytic volatilization, where the shoulder for PET/HZSM-5 (379 °C) and PET/HY (373 °C) occurs in the catalytic volatilization regime at temperatures which are close to the T_{max} of PET/H-Beta. It appears that external acid sites may be most responsible for PET catalytic volatilization, as H-Beta has the largest external surface area of all three catalysts (Table 1). It has been proposed that during the in-situ catalytic pyrolysis of PET degradation pathways can be different than the traditional 6-membered ring transition state and lead to high amounts of coke formation.[21,50] PET/H-Beta resulted in the largest solid residual (35.2%) compared with PET/HY (29.2%) and PET/HZSM-5 (17.4%). The solid residual for PET/H-Beta is likely the largest due to PET/H-Beta having the largest amount of catalytic volatilization which leads to the highest formation of coke. While HZSM-5 and HY have similar amounts of catalytic volatilization, the solid

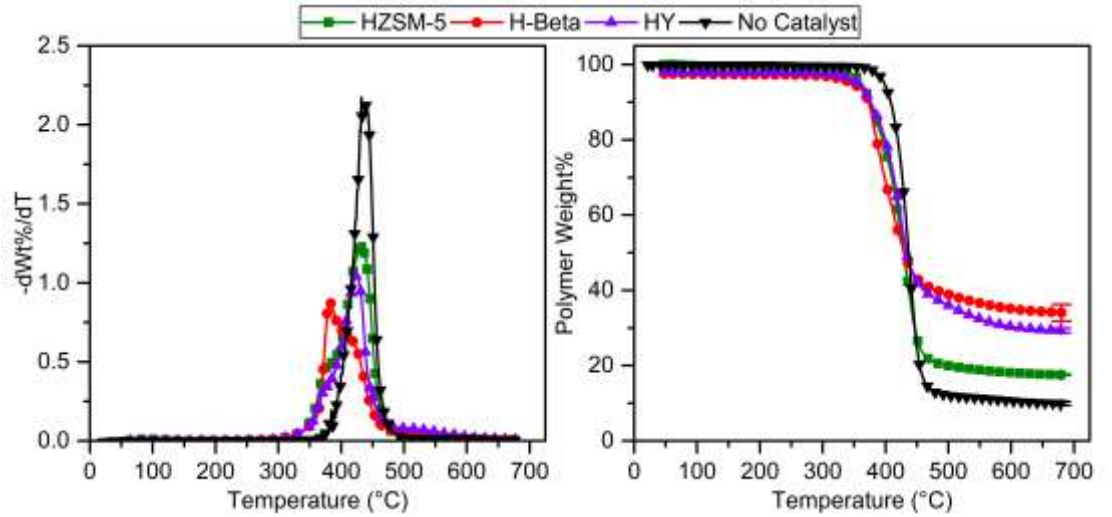

Figure 2. Derivative thermogravimetric (DTG) and polymer weight percent curves for PET pyrolysis at 10°C/min in the presence or absence of catalyst at a 1:1 catalyst to feedstock ratio

residual is likely higher for HY due its large pores allowing for the buildup of coke precursor molecules.

4.2.3 Interactions effects occurring during the catalytic co-pyrolysis of LDPE and PET

The DTG curves for the catalytic co-pyrolysis of LDPE and PET with HZSM-5, H-Beta, and HY are shown in Figure 3. An additive DTG curve for catalytic co-pyrolysis is obtained by using Eq. (29).

$$Additive\,\frac{dWt\%}{dT}_{i} = 0.5 \times \frac{dWt\%}{dT}_{PET,i} + 0.5 \times \frac{dWt\%}{dT}_{LDPE,i} \quad (29)$$

The additive DTG curve and the actual DTG curve for co-pyrolysis of LDPE and PET over the zeolites in this study is shown in Figure 3. A similar representation of these curves with the respective contributions from LDPE and PET can be seen in Figure S9. Differences are observed between the additive and the actual DTG curves for all catalysts, which clearly indicates the presence of interaction effects during the catalytic co-pyrolysis of LDPE and PET. For HZSM-5, the degradation peak for LDPE at 300 °C is much lower in magnitude for the actual co-pyrolysis curve than for the additive curve. This phenomenon is observed for all the three catalysts. The maximum value of dWt%/dT for the low temperature peak at 300-325 °C, representative of LDPE catalytic degradation during co-pyrolysis, decreased in magnitude by 40%, 12% and 27% for HZSM-5, H-Beta, and HY respectively. The presence of PET appears to delay the catalytic degradation of LDPE.

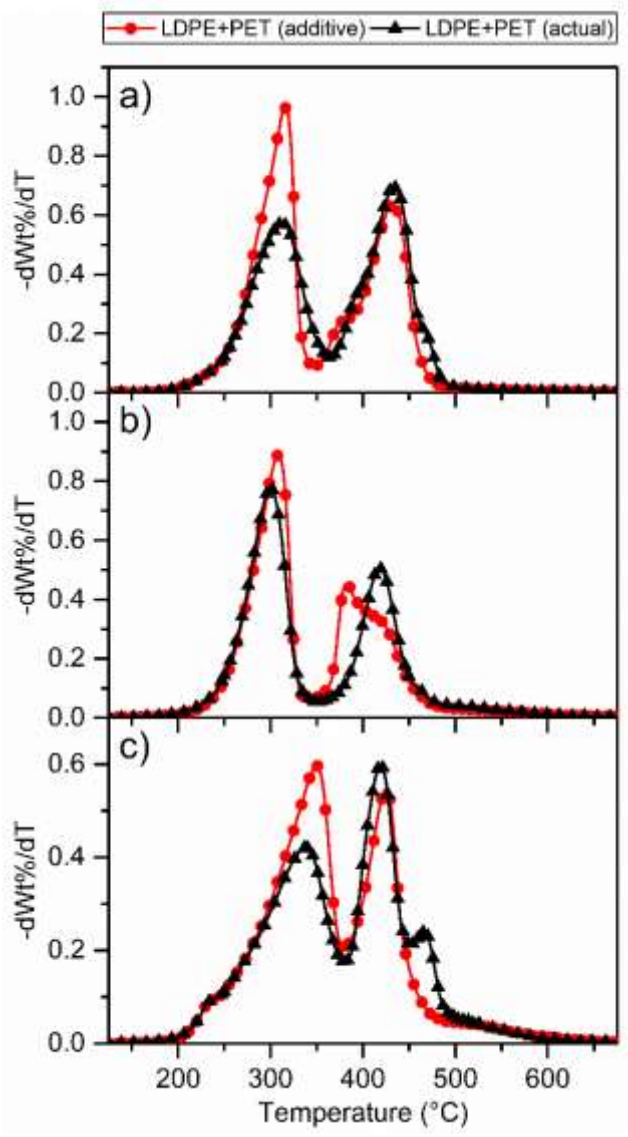

Figure 3. Comparison of additive and actual DTG curves for the catalytic co-pyrolysis of LDPE and PET with a) HZSM-5, b) H-Beta, and c) HY at 10°C/min heating rate, 1:1 LDPE:PET ratio, and 1:1 catalyst:feedstock ratio.

From Figure 3 (b), it can be observed that for H-Beta, there is a distinct shift in the temperature of maximum decomposition of PET. For the single-stream pyrolysis of PET it was observed that the T_{max} decreased from 432 °C for non-catalytic pyrolysis to 390 °C for catalytic pyrolysis with H-Beta (Figure 2). During LDPE+PET/H-Beta catalytic co-pyrolysis, T_{max} for the PET region increases to 419 °C from the 390°C observed during PET/H-Beta single-stream pyrolysis. The presence of LDPE appears to delay the catalytic degradation of PET with H-Beta catalyst. For LDPE+PET/HZSM-5 and LDPE+PET/HY the actual DTG curve is similar to the additive DTG curve for the region of PET degradation, however a high temperature shoulder at 480 °C occurs for LDPE+PET/HZSM-5 and most noticeably for LDPE+PET/HY. This shoulder is at temperatures higher than non-catalytic pyrolysis degradation and could be due to bulkier molecules exiting catalytic pores which would otherwise be left as coke at lower temperatures. An increase in conversion at temperatures of 500°C was observed by Pyra et al. during the catalytic pyrolysis of LDPE with H-Beta and was attributed to the consumption of coke deposits.[48]

4.3 Model-fitting kinetic parameters

4.3.1 Non-catalytic pyrolysis

Kinetic parameters for non-catalytic pyrolysis were derived following the approach outlined in Section 3 using three experimental curves in the objective function: LDPE, PET, and LDPE+PET. LDPE and PET were both pyrolyzed non-catalytically at three different heating rates of 5, 10, and 50 °C/min so that isoconversional approach could estimate activation energy and pre-exponential factor via the Flynn-Wall-Ozawa method (FWO). The procedure for obtaining these parameters via FWO method are described in Section S2 of the Supplementary Information. The parameters obtained for various conversions and the corresponding regression coefficient (R^2) values are shown in Table S1. The FWO method resulted in activation energy and pre-exponential factor of 227.9 ± 1.4 kJ/mol and

Table 2. Kinetic parameters obtained for the non-catalytic degradation of LDPE and PET and the corresponding fit% for LDPE, PET, and LDPE+PET. A (s-1) and E (kJ/mol)

LDPE kinetic parameters		PET kinetic parameters	
$A_{NC,L}$	6.344E16	$A_{NC,P}$	7.486E18
$E_{NC,L}$	268.2	$E_{NC,P}$	283.0
$n_{NC,L}$	0.788	$n_{NC,P}$	1.359
		γ	0.893
$Fit\%_{Wt\%}$		$Fit\%_{DTG}$	
LDPE	99.32	LDPE	98.88
PET	99.38	PET	97.80
LDPE+PET	99.48	LDPE+PET	97.84

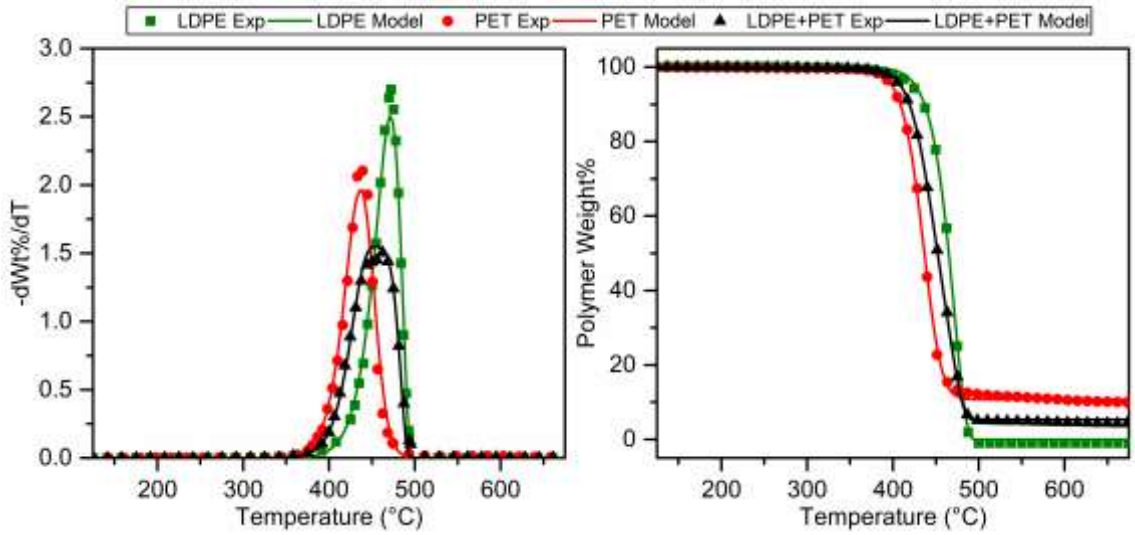

Figure 4. Experimental and model DTG and polymer weight% curves for the non-catalytic pyrolysis of LDPE, PET, and LDPE+PET at a 1:1 ratio with a heating rate of 10 °C/min

8.18 x 10^{13} s^{-1} for LDPE and 203.9 ± 5.5 kJ/mol and 8.65 x 10^{12} s^{-1} for PET. These values for activation energy of LDPE and PET are in line with those reported in the literature.[27,51]

The activation energy and pre-exponential values obtained for LDPE and PET via FWO method were used as initial guesses for the n^{th} order reaction scheme, along with $n_{NC,L}$ and $n_{NC,P}$ both equal to 1 and γ = 0.9. The boundary conditions of 5 < log(A) < 30, 50 < E < 350, 0.01 < n < 10, and 0 < γ < 1 were input into the solver. During non-catalytic pyrolysis, LDPE and PET show only a low level of interaction effects (Figure S10). Thus, one set of kinetic parameters was able to model well both the single stream and co-pyrolysis of LDPE and PET. The obtained kinetic parameters from the optimization and the corresponding Fit% values for LDPE, PET, and LDPE+PET can be seen in Table 2. The parameters deviated significantly from their initial guesses determined via FWO approach. This is most likely due to the initial guesses being derived assuming 1st order

reaction mechanism when using FWO approach, where the reaction scheme using the least squares fitting is n^{th} order and allows for varying of reaction order from 0.1 to 3. It has been reported in the literature that when modeling biomass pyrolysis via an independent parallel reaction scheme, that allowing reactions to go from being 1st order to n^{th} order will improve Fit%, while also changing substantially the activation energy and pre-exponential factor.[31]

4.3.2 Catalytic pyrolysis

The experimental mass loss data obtained from the catalytic pyrolysis of LDPE, PET, and LDPE+PET with HZSM-5, H-Beta, and HY was used to evaluate kinetic parameters for catalytic pyrolysis. In the proposed reaction scheme (R1)-(R4), LDPE and PET can decompose both catalytically and non-catalytically. The catalyst to feedstock ratio, the coefficients *a* and *b*, and the difference in the kinetic triplet for non-catalytic and catalytic pyrolysis, all play a pivotal role in how much the polymer is degraded via catalytic routes as opposed to non-catalytic routes.

It is worthwhile to mention that to keep consistency throughout, the non-catalytic pyrolysis parameters obtained in section 4.3.1 are used for catalytic experiments and are not allowed to vary while optimizing the parameters for catalytic pyrolysis. The boundary conditions for *A, E*, and *n* are kept the

Table 3. Kinetic parameters obtained for the catalytic degradation of LDPE and PET over zeolite catalysts and the corresponding fit% for LDPE, PET, and LDPE+PET catalytic pyrolysis experiments. A (s^{-1}) and E (kJ/mol)

LDPE kinetic parameters				PET kinetic parameters			
	HZSM-5	H-Beta	HY		HZSM-5	H-Beta	HY
$A_{C,L1}$	8.971E10	3.368E10	7.899E9	$A_{C,P1}$	5.473E9	3.749E6	1.877E10
$E_{C,L1}$	106.7	120.2	101.0	$E_{C,P1}$	112.5	110.1	110.0
$n_{C,L1\_L}$	2.505	2.507	0.987	$n_{C,P1\_P}$	3.107	1.214	0.900
$n_{C,L1\_C}$	5.090	1.801	2.092	$n_{C,P1\_C}$	1.941	1.220	2.187
$A_{C,L2}$	1.139E8	1.263E8	6.291E5	$A_{C,P2}$	2.515E10	3.061E6	1.438E8
$E_{C,L2}$	116.0	115.0	96.9	$E_{C,P2}$	170.8	105.0	144.9
$n_{C,L2}$	1.010	0.956	3.193	$n_{C,P2}$	5.459	3.311	2.430
a	0.672	2.347	4.151	b	5.112	0.469	1.797
α	0.985	0.904	0.885	β	0.821	0.619	0.687
$Fit\%_{Wt\%}$				$Fit\%_{DTG}$			
LDPE	98.93	97.51	96.08	LDPE	96.24	97.54	96.43
PET	98.74	97.12	98.33	PET	97.13	96.19	96.85
LDPE+PET	98.97	99.00	98.32	LDPE+PET	95.44	96.36	94.18

same as mentioned in section 4.3.1. The coke formation coefficients α and β were allowed to vary from 0 to 1, and the polymer to catalyst coefficients *a* and *b* from 0.01 to 10. An optimization of kinetic parameters was carried out such that the error between experimental data points and the model is minimized. The resulting kinetic parameters determined from the optimization can be seen in Table 3, and the resulting model curves which arise from the obtained kinetic parameters can be seen compared with the experimental curves in Figure 5.

A combination of the non-catalytic kinetic parameters in Table 2 and the catalytic kinetic parameters in Table 3 were able to model LDPE catalytic pyrolysis, PET catalytic pyrolysis, and LDPE+PET catalytic co-pyrolysis for HZSM-5, H-Beta, and HY catalyst with $Fit\%_{Wt\%} > 96$ and $Fit\%_{DTG} > 93$ for all experimental curves. The kinetic parameters used to model the single-stream catalytic pyrolysis were the same that were used to model the catalytic co-pyrolysis for a given catalyst. To the authors knowledge, this is the first time one set of kinetic parameters were used to model both the single-stream and co-pyrolysis of multiple polymers in the presence of a catalyst.

Interaction effects observed during catalytic co-pyrolysis which can be seen in Figure 3 are able to be modeled using the proposed reaction scheme, which allows both LDPE and PET to bind to the catalyst forming the complexes LDPEC and PETC. For instance, when looking at Figure 3a it can be observed that for HZSM-5, the LDPE+PET (actual) curve is only 60% in magnitude of what would be expected at a temperature of 300 °C. It can be seen in Figure 5a that the kinetic parameters for HZSM-5 allowed for both a higher magnitude of degradation for LDPE and a decreased magnitude for LDPE+PET at 300 °C. For HZSM-5, the optimized values for the coefficient *b* which represents the grams of catalyst needed to react with a gram of PET to form the complex PETC was 5.112, while the corresponding coefficient *a* for LDPE was 0.672. These results demonstrate the fact that PET saturates the catalyst in the reaction model due to the high *b* coefficient value, thus delaying the catalytic degradation of LDPE at 300 °C while in the presence of PET. Interaction effects were also modeled for H-Beta catalyst. In Figure 3b, it can be seen that T_{max} for PET degradation shifts from 390 °C for single-stream pyrolysis to 419°C during co-pyrolysis. The model resulted in a shift of T_{max} of 396°C for single-stream pyrolysis to 412°C for co-pyrolysis. For H-Beta, the optimized value for *a* was 2.347, and for *b* was 0.469. This value of *a* which was larger than *b* allowed LDPE to decrease the available catalytic sites thus leading to a delayed catalytic degradation for PET. The n^{th} order reaction scheme with the

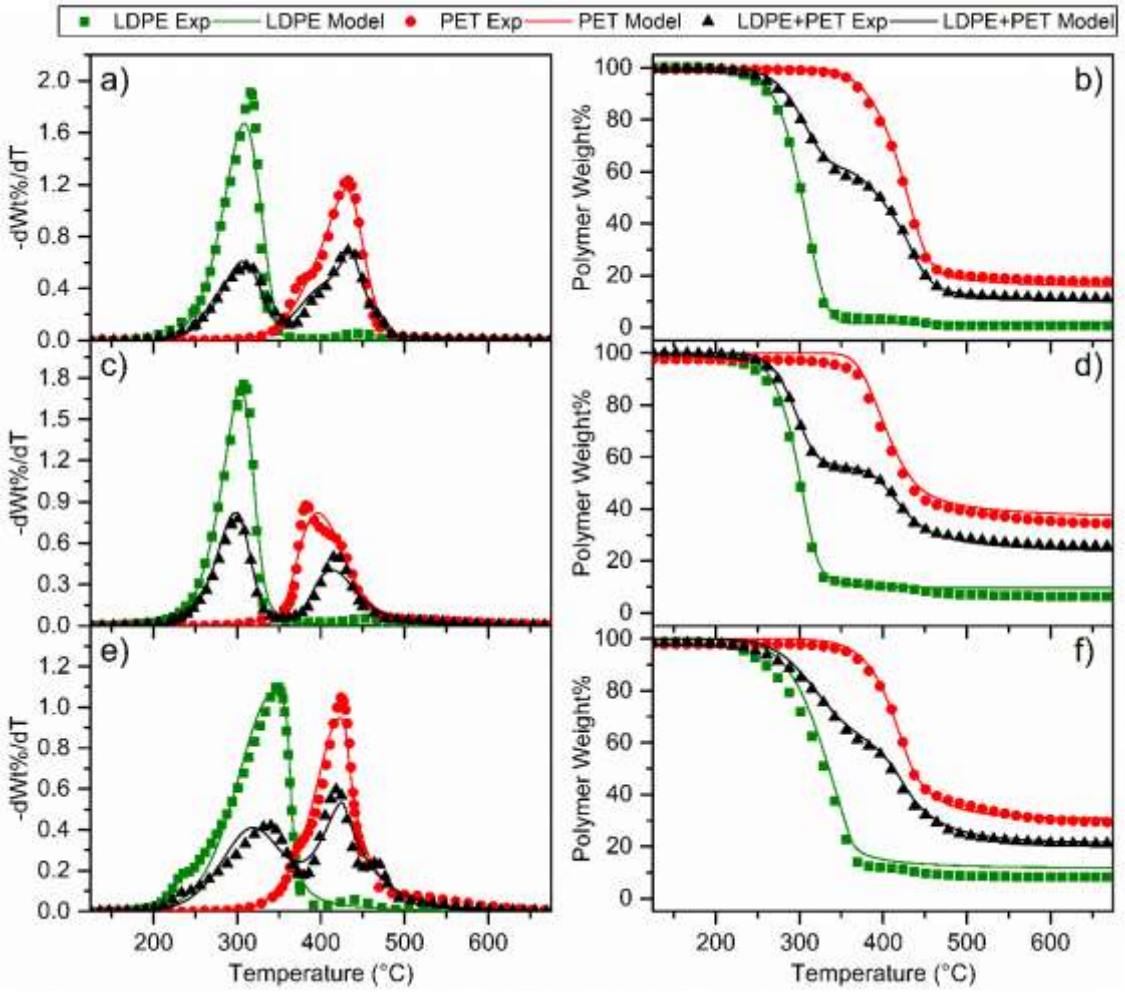

Figure 5. Experimental and model DTG and polymer weight% curves for the catalytic pyrolysis of LDPE, PET, and LDPE+PET with HZSM-5 (a, b), H-Beta (c, d), and HY (e, f)

implemented boundary conditions resulted in a comparatively low Fit%$_{DTG}$ of 93.77% for LDPE/HY. It can be seen in Figure 1 that LDPE/HY has a markedly different DTG curve than for LDPE/HZSM-5 and LDPE/H-Beta. The challenge for the reaction scheme to accurately model the elongated DTG peak for LDPE/HY, also resulted in a relatively low Fit%$_{DTG}$ for LDPE+PET/HY of 93.29%.

4.4 Catalytic pyrolysis of LDPE and PET in a Pyroprobe® micro-reactor (Py-GC/MS)

4.4.1 LDPE catalytic pyrolysis

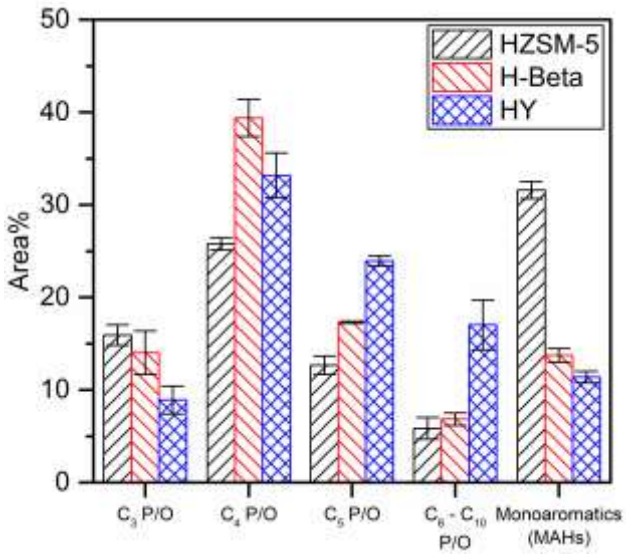

Figure 6. Py-GC/MS area% of C_3-C_{10} paraffins and olefins (P/O) and aromatic compounds formed during the catalytic pyrolysis of LDPE at 500 °C over various zeolite catalysts at 10:1 catalyst to feedstock ratio

Figure 6 depicts the GC/MS area% of main pyrolysis products formed during the catalytic fast pyrolysis of LDPE with various zeolites. A complete list of identified compounds with their corresponding area% can be found in Table S2. The total ion chromatogram (TIC) plots for LDPE catalytic Py/GC-MS experiments can be seen in Figure S11. For LDPE catalytic pyrolysis, C_3-C_{10} paraffins and olefins and single ring aromatic compounds are the main pyrolysis products and make up 91.7, 91.8, and 94.4% of the total area% for pyrolysis with HZSM-5, H-Beta, and HY, respectively. It can be observed that HZSM-5 with the smallest pore size forms the most C_3 paraffins and olefins, H-Beta with the medium pore size forms the most C_4 paraffins and olefins, and HY with the largest pore size forms the most C_5-C_{10} paraffins and olefins. A similar trend was observed by Elordi et al. during the continuous fast pyrolysis of HDPE with HZSM-5, H-Beta, and HY in a conical spouted bed reactor at 500°C.[19] In our study, it was observed that HZSM-5 resulted in the largest area% of aromatic compounds (31.6%) compared with H-Beta and HY (13.7% and 11.4%, respectively). These results are in line with Xue et al. who reported a high carbon yield% of aromatic compounds (26.55%) for PE/HZSM-5 during in-situ catalytic pyrolysis in a micro-reactor at 600 °C.[21] Besides, Li et al. also reported a single-ring aromatic yield% of 31% for LDPE/HZSM-5 fast pyrolysis in a Pyroprobe® reactor at 650 °C.[52] The yield of aromatics reported by Elordi et al. did not vary significantly between HZSM-5, H-Beta, and HY catalyst, with yield of aromatics being in the range of 5-12% for all the three catalysts. The incongruencies in the yields of the products obtained by various authors for polyethylene pyrolysis can be primarily due to different reactor types and pyrolysis temperatures used for their studies.

4.4.2 PET Catalytic Pyrolysis

The GC/MS area% for the main products formed during the catalytic pyrolysis of PET with various zeolites is shown in Figure 7. A complete list of identified compounds with their corresponding area% can be found in Table S3. The TIC plots for PET catalytic Py/GC-MS experiments can be seen in Figure S12.

It is known that acid sites on zeolite catalysts help to decarboxylate terephthalic acid and benzoic acid, which are main products from PET non-catalytic pyrolysis, thus forming large amounts of benzene.[21,23] It is seen that H-Beta and HY result in slightly higher area% of benzene (55.7% and 54.4%) compared to HZSM-5 (43.5%). The observed area% of polyaromatics is substantially higher with HZSM-5 (24.7%) compared to that observed with H-Beta and HY (10.1% and 5.9%). It is likely that the larger pore size of H-Beta and HY allow for polyaromatic compounds formed via condensation reactions to further condense into larger polyaromatics which eventually lead to formation of coke, thus decreasing the selectivity to polyaromatics for these catalysts. This can be substantiated by the fact that higher selectivity to three ring and four ring polyaromatics such as phenanthrene and pyrene was observed for H-Beta and HY (Table S3).

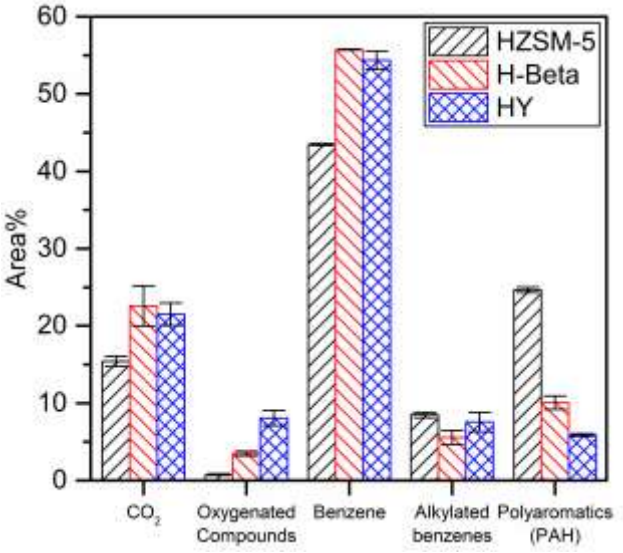

Figure 7. Py-GC/MS area% of various compounds formed during the catalytic pyrolysis of PET at 500 °C over various zeolite catalysts at 10:1 catalyst to feedstock ratio

Another notable trend that can be observed from Figure 7 is that the area% of oxygenated compounds is highest for HY and lowest for HZSM-5. Other studies have shown that HZSM-5 with high acid strength and Brønsted : Lewis acid ratio had higher deoxygenation capabilities for bio-oil oxygenates than for HY,[53] which coincides with the results observed in our study. The oxygenated compound with the highest area% for all catalysts

was acetaldehyde, which resulted in an area% of 0.52%, 3.02%, and 7.52% for HZSM-5, H-Beta, and HY respectively. Interestingly the area% for benzoic acid did not follow a similar trend, where benzoic acid area% was 0.09%, 0.15% and 0.06% for HZSM-5, H-Beta, and HY respectively. It could be that the Lewis acid sites present in H-Beta and HY favor decarbonylation over decarboxylation reaction pathways which leads to increased amounts of acetaldehyde.[54] This is supported by the fact that H-Beta and HY form higher amounts of benzaldehyde (0.09% and 0.32%) than for HZSM-5 (0.03%), as the proposed reaction pathway for formation of acetaldehyde produces benzaldehyde as a reaction intermediate, as seen in Figure 9.

4.4.3 LDPE+PET Catalytic Co-Pyrolysis

The area% of main products formed during the co-pyrolysis of LDPE and PET are shown in Figure 8 (a). A complete list of identified compounds with their corresponding area% can be found in Table S4. The TIC plots for LDPE and PET catalytic co-pyrolysis experiments (Py/GC-MS) can be seen in Figure S13. During co-pyrolysis a strong co-elution between acetaldehyde and C_4 products was observed during chromatography and thus area% of the two were lumped together. Figure 8 (b) depicts the synergy% of the main products. Synergy% > 0 implies that the product formed during co-pyrolysis is more than that expected from the product distribution obtained from single-stream experiments. It can be observed that for all the three catalysts, there is a negative synergy for C_4-C_{10} paraffins and olefins and benzene, and a positive synergy for alkylated benzenes and polyaromatic hydrocarbons. An increase in the actual yield% of alkylated benzenes such as toluene and xylene was observed by Xue et al. during the catalytic co-pyrolysis of PE and PET with HZSM-5.[21] The results obtained in this work are in line with that of Xue et al. An increased amount of alkylated benzenes is observed in this work. It can be thus proposed that paraffins and olefins produced from LDPE undergo alkylation reactions with benzene and phenyl radicals produced from PET leading to increased amounts of alkylated benzenes.[55] The alkylated benzene synergy% for the catalysts is as follows: HY (142%) > H-Beta (44.1%) > HZSM-5 (3.06%). HY having the highest synergy% for alkylated benzenes can be attributed to the low Brønsted : Lewis acid ratio of HY (1.1:1). Other works have shown that a higher synergy% for alkylated benzenes is observed during polyethylene-cellulose catalytic co-pyrolysis when iron is introduced to ZSM-5 catalyst, thus giving the catalyst a lower Brønsted : Lewis acid ratio.[56] This reasoning corresponds well with our findings, as H-Beta which had moderate Brønsted : Lewis acid ratio (5.3:1) had moderate synergy% for alkylated benzenes, and HZSM-5 which had high Brønsted : Lewis acid (80.5:1) ratio had the lowest synergy% for alkylated benzenes.

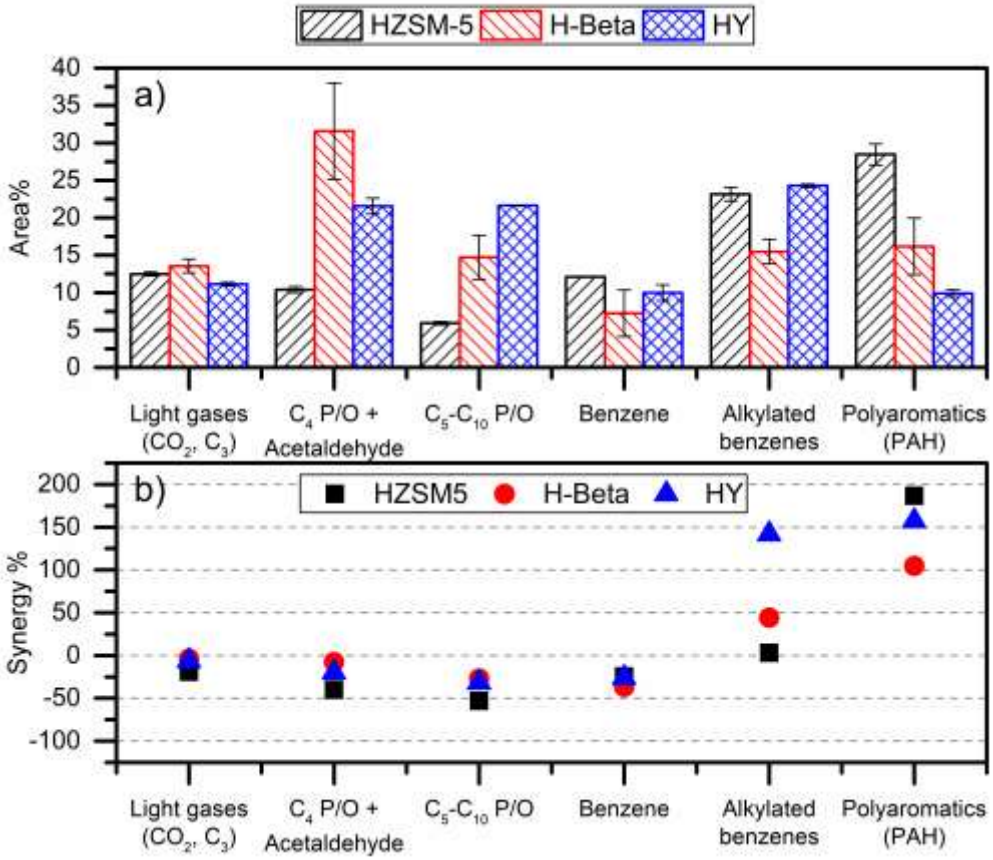

Figure 8. GC/MS area% of light gases (CO_2 and C3 paraffins and olefins (P/O)), C_4 P/O and acetaldehyde, C_5-C_{10} P/O , benzene, alkylated benzenes, and polyaromatic hydrocarbons formed during the catalytic co-pyrolysis of LDPE and PET over various zeolites (a), and the synergy% of these products, which measures the increase or decrease of these products from what would be expected (b)

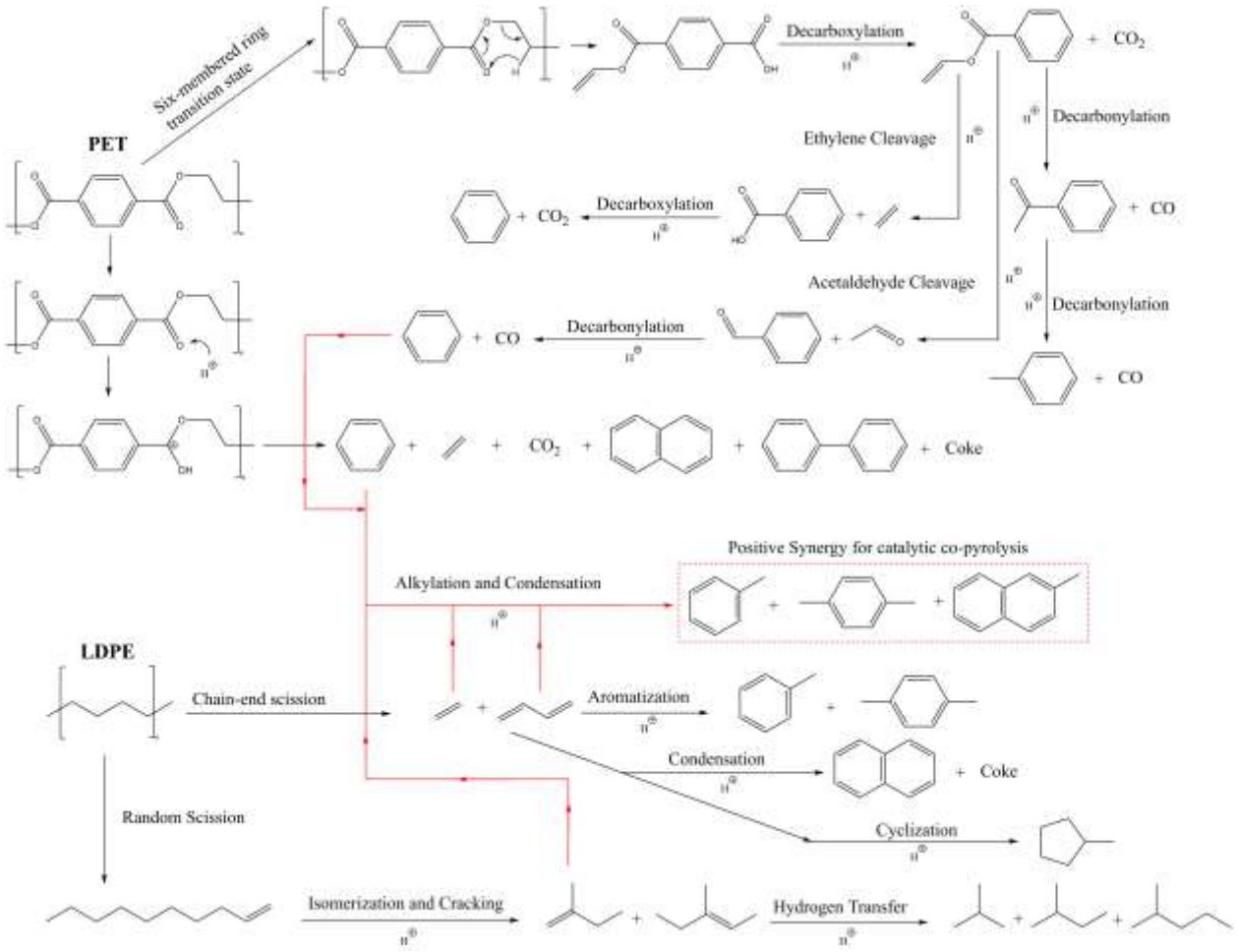

Figure 9. Plausible reaction pathways for the catalytic co-pyrolysis of LDPE and PET with zeolite acid catalysts

Alkylated benzenes can be useful for liquid fuels as they act as octane boosters.[57] The content of benzene is to be minimized in fuel,[58] so an interaction effect which decreases benzene and increases alkylated benzenes would be desirable when pyrolyzing plastic waste for fuel. HY shows to be the most attractive catalyst out of the three for producing liquid fuels such as gasoline. This is because HY has the highest area% of C_5-C_{10} paraffins along with the highest positive synergy% for valuable alkylated benzenes and a concomitant negative synergy% for benzene.

In addition to alkylated benzenes, a positive synergy% was also observed for polyaromatics hydrocarbons for all catalysts. It is known that phenyl radicals which arise from PET pyrolysis could react with branched olefins to produce naphthalenes.[59] The synergy% for polyaromatics is highest for HZSM-5 and this could be possibly due to pyrolysis of LDPE with HZSM-5 being known to produce a large amount of olefins.[17] The negative synergy% for benzene and C_4-C_{10} paraffins and olefins is almost equal for all catalysts, however the type of zeolite seems to strongly favor the positive synergy% of alkylated benzenes and polyaromatics which is observed. HZSM-5 gives a large increase in polyaromatics and close to no increase in alkylated benzenes. On the other hand, HY showed a large increase and H-Beta showed a moderate increase in the synergy% of both polyaromatics and alkylated benzenes.

The plausible reaction pathways leading to the formation of main products during the catalytic fast pyrolysis and co-pyrolysis of LDPE and PET are depicted in Figure 9. Since the three catalysts used in this study are all zeolite acid catalysts, the reaction pathways delineated in Figure 9 apply for all. The characteristics of the acid catalysts such as pore size, total acidity, acid strength, and Brønsted : Lewis acid ratio can control the reaction pathways which are dominant, thus altering the final product distribution.

For PET, it was mentioned in section 4.2.2 that the volatilization seems to occur both catalytically and non-catalytically when pyrolyzed in the presence of catalyst. The non-catalytic volatilization can to occur via a six-membered cyclic transition state in which a β-hydrogen atom is transferred to double bonded oxygen while the C-O bond is cleaved, resulting in the formation of carboxylic acid and vinyl end groups.[16,60,61] After initial pyrolysis volatiles form, acid catalysts can then aid in the decarboxylation of carboxylic end groups,[62] leading to the production of vinyl benzoate. Vinyl benzoate acts as an intermediate which can go through multiple reaction pathways, either undergoing decarbonylation for production of acetophenone, ethylene cleavage for production of benzoic acid, or acetaldehyde cleavage for production of benzaldehyde.[16] Benzoic acid can undergo further decarboxylation for production of benzene. Acetophenone and

benzaldehyde undergo further decarbonylation for the production of toluene and benzene respectively.[21,50] It can be observed in Table S3 that HY, which resulted in the highest selectivity to acetaldehyde (7.52%) of all the three catalysts, also had the highest selectivity to benzaldehyde (0.32%). This supports the proposed reaction pathway which leads to the concurrent production of benzaldehyde and acetaldehyde.

In addition to non-catalytic volatilization occurring via the six-membered cyclic transition state, catalytic volatilization has been proposed to occur via the C=O bond of PET being attacked by external protons on zeolite acid sites, ultimately leading to the formation of phenyl radicals.[21] The phenyl radicals can undergo recombination reactions for the production of benzene and polyaromatic hydrocarbons such as biphenyl and naphthalene.[50,63,64] It is well-known that polyaromatic compounds act as coke precursor molecules,[36] and this explains the high solid residual% observed during PET catalytic TGA experiments shown in Figure 2, and the high solid residual% observed by others during the in-situ catalytic pyrolysis of PET.[21] Ethylene and CO_2 are proposed to be produced alongside benzene and polyaromatics via the catalytic volatilization pathway.[21,50]

For the degradation of LDPE, either random scission or chain scission can occur producing either smaller olefins or larger olefins respectively.[65,66] The light olefins from end chain cracking can either undergo dehydrocyclization for production of aromatics, condensation reactions for production of polyaromatics and coke, or cyclization for production of cycloalkanes.[65–67] The larger olefins formed from random scission can interact with catalytic acid sites which provide the proton source for C=C bonds to yield carbonium ions. The presence of carbonium ions leads to isomerization and cracking reactions for the formation of branched paraffins and olefins.[68,69] During the catalytic co-pyrolysis of LDPE and PET, interactions were quite evident that resulted in a decrease in selectivity to benzene and C_4-C_{10} paraffins and olefins with concomitant increase in selectivity to alkylated benzenes and polyaromatics. It can be speculated that the paraffins and olefins react with either benzene or phenyl radicals via condensation and alkylation reactions, thereby increasing the selectivity to alkylated benzenes and polyaromatics. This is in accordance with the increase in alkylated benzenes during PE/PET catalytic co-pyrolysis with HZSM-5,[21] as well as the proposed mechanism for benzene reacting with cracked LDPE chains to form substituted benzenes during the catalytic cracking of LDPE dissolved in benzene over HZSM-5.[70] It is known that phenyl radicals will react with light olefins such as propene to form alkylated benzenes and polycyclic hydrocarbons such as indene,[71] and that benzene will undergo alkylation reactions with light olefins in the presence of zeolite catalysts.[55]

Conclusions

The presence of catalyst decreases the degradation temperature for LDPE to a much greater extent for LDPE than for PET. For LDPE, the T_{max} decreased by 158, 160, and 128 °C for HZSM-5, H-Beta, and HY, respectively. For PET the T_{max} decreased 0, 42, and 6 °C for HZSM-5, H-Beta, and HY. Interaction effects were observed in the DTG curves during the catalytic co-pyrolysis of LDPE and PET for all catalysts studied. For all the catalysts, a decrease in the extent of the degradation of LDPE at 300 °C was observed, which implies that the presence of PET delays the catalytic degradation of LDPE. A lumped reaction scheme was able to model both the non-catalytic and the catalytic pyrolysis of LDPE, PET, and LDPE+PET mixture. The reaction scheme was able to capture the interaction effects present during catalytic co-pyrolysis via competitive binding to catalytic active sites between the two polymers. A single set of kinetic parameters was shown to model well for both the single-stream pyrolysis of LDPE and PET and the co-pyrolysis of LDPE and PET. The fast catalytic pyrolysis of LDPE in a Pyroprobe® micro-reactor showed that the zeolite framework which was used had an effect on the selectivity to light paraffins and olefins (C_3-C_4), gasoline range paraffins and olefins (C_5-C_{10}), and aromatic compounds. A high selectivity to benzene was seen for all catalysts during the fast pyrolysis of PET. During catalytic co-pyrolysis of LDPE and PET, an interaction effect where the selectivity of alkylated benzenes and polyaromatics was greater than expected and the selectivity of benzene and C_4-C_{10} paraffins and olefins was less than expected. HY led to the largest increase in alkylated benzenes during the co-pyrolysis of LDPE and PET and resulted in the highest area% of C_5-C_{10} paraffins and olefins. The high production of these gasoline range paraffins and olefins along with an increase in production of octane-boosting alkylated benzenes shows that HY could be a potential catalyst for converting mixed LDPE and PET waste into valuable liquid fuels.

Conflicts of interest

There are no conflicts to declare.

Acknowledgements

This material is based upon work supported by the U.S. Department of Energy's Office of Energy Efficiency and Renewable Energy (EERE) under the Advanced Manufacturing Office Award Number DE-EE0007897" awarded to the REMADE Institute, a division of Sustainable Manufacturing Innovation Alliance Corp. This report was prepared as an account of work sponsored by an agency of the United States Government. Neither the United States Government nor any agency thereof, nor any of their employees, makes any warranty, express or implied, or assumes any legal liability or responsibility for the accuracy, completeness, or usefulness of any information, apparatus, product, or process disclosed, or represents that its use would not infringe privately owned rights. Reference herein to any specific commercial product, process, or service by trade name, trademark, manufacturer, or otherwise does not necessarily constitute or imply its endorsement, recommendation, or favoring by the United States Government or any agency thereof. The views and opinions of authors expressed herein do not necessarily state or reflect those of the

United States Government or any agency thereof. This material was supported by the Penn State Energy and Environmental Sustainability Laboratory (EESL) 2021 Green award. The authors thank Dr. Ozge Bozkurt for useful discussions and input. The authors thank Prof. Robert Rioux and Prof. Phillip Savage for providing access to TGA equipment.

References

1 R. Geyer, J. R. Jambeck and K. L. Law, *Sci. Adv.*, 2017, **3**, 25–29.
2 J. G. B. Derraik, *Mar. Pollut. Bull.*, 2002, **44**, 842–852.
3 D. E. MacArthur, D. Waughray and M. R. Stuchtey, 2016, 1–120.
4 M. Biron, *A Practical Guide to Plastics Sustainability*, Elsevier, 2020.
5 K. Ragaert, L. Delva and K. Van Geem, *Waste Manag.*, 2017, **69**, 24–58.
6 NAPCOR (National Association for PET Container), 2018, 3.
7 Ellen MacArthur Foundation, *Ellen MacArthur Found.*, 2017, 1–150.
8 O. Horodytska, F. J. Valdés and A. Fullana, *Waste Manag.*, 2018, **77**, 413–425.
9 K. Sivagami, G. Divyapriya and R. Selvaraj, *Process Saf. Environ. Prot.*, 2021, **149**, 497–506.
10 A. H. Tullo, *Chem. Eng. News*, 2019, 97, 29–34.
11 G. Lopez, M. Artetxe, M. Amutio, J. Bilbao and M. Olazar, *Renew. Sustain. Energy Rev.*, 2017, **73**, 346–368.
12 X. Zhou, L. J. Broadbelt and R. Vinu, *Mechanistic Understanding of Thermochemical Conversion of Polymers and Lignocellulosic Biomass*, Elsevier Inc., 1st edn., 2016, vol. 49.
13 P. T. Williams and E. A. Williams, *J. Anal. Appl. Pyrolysis*, 1999, **51**, 107–126.
14 T. Yoshioka, G. Grause, C. Eger, W. Kaminsky and A. Okuwaki, *Polym. Degrad. Stab.*, 2004, **86**, 499–504.
15 M. Artetxe, G. Lopez, M. Amutio, G. Elordi, M. Olazar and J. Bilbao, *Ind. Eng. Chem. Res.*, 2010, **49**, 2064–2069.
16 A. Dhahak, C. Grimmer, A. Neumann, C. Rüger, M. Sklorz, T. Streibel, R. Zimmermann, G. Mauviel and V. Burkle-Vitzthum, *Waste Manag.*, 2020, **106**, 226–239.
17 G. Elordi, M. Olazar, M. Artetxe, P. Castaño and J. Bilbao, *Appl. Catal. A Gen.*, 2012, **415**–**416**, 89–95.
18 G. Manos, A. Garforth and J. Dwyer, *Ind. Eng. Chem. Res.*, 2000, **39**, 1198–1202.
19 G. Elordi, M. Olazar, G. Lopez, M. Amutio, M. Artetxe, R. Aguado and J. Bilbao, *J. Anal. Appl. Pyrolysis*, 2009, **85**, 345–351.
20 G. Elordi, M. Olazar, G. Lopez, P. Castaño and J. Bilbao, *Appl. Catal. B Environ.*, 2011, **102**, 224–231.
21 Y. Xue, P. Johnston and X. Bai, *Energy Convers. Manag.*, 2017, **142**, 441–451.
22 H. Lee, Y.-M. Kim, S.-C. Jung and Y.-K. Park, *J. Nanosci. Nanotechnol.*, 2020, **20**, 5594–5598.
23 S. Du, J. A. Valla, R. S. Parnas and G. M. Bollas, *ACS Sustain. Chem. Eng.*, 2016, **4**, 2852–2860.
24 A. Y. Snegirev, M. K. Handawy, V. V. Stepanov and V. A. Talalov, *Polym. Degrad. Stab.*, 2019, **161**, 245–259.
25 M. Al-Asadi and N. Miskolczi, *IOP Conf. Ser. Earth Environ. Sci.*, , DOI:10.1088/1755-1315/154/1/012021.
26 M. Al-Asadi, L. Gombor and N. Miskolczi, *Chem. Eng. Trans.*, 2018, **70**, 1663–1668.
27 A. Aboulkas, K. El harfi and A. El Bouadili, *Energy Convers. Manag.*, 2010, **51**, 1363–1369.
28 V. Mortezaeikia, O. Tavakoli and M. S. Khodaparasti, *J. Anal. Appl. Pyrolysis*, 2021, **160**, 105340.
29 A. Marcilla, A. Gómez-Siurana and F. Valdés, *Polym. Degrad. Stab.*, 2007, **92**, 197–204.
30 T. Anh, H. Vu, Q. Khanh, B. Kwon, S. Kim and J. Kim, *Energy Convers. Manag.*, 2021, **249**, 114879.
31 A. Anca-couce, A. Berger and N. Zobel, *Fuel*, 2014, **123**, 230–240.
32 H. Liu, M. S. Ahmad, H. Alhumade, A. Elkamel, S. Sammak and B. Shen, *Energy Convers. Manag.*, 2020, **208**, 112531.
33 T. M. Kruse, S. E. Levine, H. Wong, E. Duoss, A. H. Lebovitz, J. M. Torkelson and L. J. Broadbelt, *J. Anal. Appl. Pyrolysis*, 2005, **73**, 342–354.
34 T. Faravelli, G. Bozzano, M. Colombo, E. Ranzi and M. Dente, *J. Anal. Appl. Pyrolysis*, 2003, **70**, 761–777.
35 B. C. Lippens and J. H. De Boer, *J. Catal.*, 1965, **4**, 319–323.
36 Z. Chen, X. Zhang, F. Yang, H. Peng, X. Zhang, S. Zhu and L. Che, *Appl. Catal. A, Gen.*, 2021, **609**, 117873.
37 F. Jiang, L. Zeng, S. Li, G. Liu, S. Wang and J. Gong, *ACS Catal.*, 2014, **5**, 438–447.
38 A. I. Osman, J. K. Abu-dahrieh, D. W. Rooney, S. A. Halawy, M. A. Mohamed and A. Abdelkader, *Appl. Catal. B, Environ.*, 2012, **127**, 307–315.
39 C. A. EMEIS, *J. Catal.*, 1993, **141**, 347–354.
40 J. V. Jayarama Krishna, O. P. Korobeinichev and R. Vinu, *J. Anal. Appl. Pyrolysis*, 2019, **139**, 48–58.
41 A. Marcilla, M. I. Beltrán, A. Gómez-Siurana, R. Navarro and F. Valdés, *Appl. Catal. A Gen.*, 2007, **328**, 124–131.
42 J. V. J. Krishna, S. S. Damir and R. Vinu, *J. Environ. Chem. Eng.*, 2021, **9**, 105382.
43 T. Ennaert, J. Geboers, E. Gobechiya, C. M. Courtin, M. Kurttepeli, K. Houthoofd, C. E. A. Kirschhock, P. C. M. M. Magusin, S. Bals, P. A. Jacobs and B. F. Sels, *ACS Catal.*, 2015, 754–768.
44 M. Ravi, V. L. Sushkevich and J. A. van Bokhoven, *Nat. Mater.*, 2020, **19**, 1047–1056.
45 D. P. Serrano, J. Aguado and J. M. Escola, *J. Anal. Appl. Pyrolysis*, 2005, **74**, 353–360.
46 J. Agullo, N. Kumar, D. Berenguer, D. Kubicka, A. Marcilla, A. Gómez, T. Salmi and D. Y. Murzin, *Kinet. Catal.*, 2007, **48**, 535–540.
47 M. M. Hasan, N. Batalha, G. Fraga, M. H. M. Ahmed, L. Pinard, M. Konarova, S. Pratt and B. Laycock, *Sustain. Energy Fuels*, 2022, **6**, 1587–1602.
48 K. Pyra, K. A. Tarach, A. Śrębowata, I. Melián-cabrera and K. Góra-marek, *Appl. Catal. B Environ.*, 2020, **277**, 119070.
49 S. Patnaik, A. K. Barick and K. A. Panda, *Prog. Rubber, Plast. Recycl. Technol.*, 2021, **37**, 148–164.
50 H. Jia, H. Ben, Y. Luo and R. Wang, *Polymers (Basel).*, 2020, **12**, 705.

51 R. K. Mishra, A. Sahoo and K. Mohanty, *Bioresour. Technol.*, 2019, **289**, 121608.
52 X. Li, H. Zhang, J. Li, L. Su, J. Zuo, S. Komarneni and Y. Wang, *Appl. Catal. A Gen.*, 2013, **455**, 114–121.
53 B. Valle, R. Palos, J. Bilbao and A. G. Gayubo, *Fuel Process. Technol.*, 2022, **227**, 107130.
54 M. E. Sad, L. F. González Peña, C. L. Padró and C. R. Apesteguía, *Catal. Today*, 2018, **302**, 203–209.
55 A. Corma, V. Martínez-Soria and E. Schnoeveld, *J. Catal.*, 2000, **192**, 163–173.
56 J. Wang, J. Jiang, Y. Sun, X. Meng, X. Wang, R. Ruan, A. J. Ragauskas and D. C. W. Tsang, *J. Hazard. Mater.*, 2021, **414**, 125418.
57 A. Demirbas, M. A. Balubaid, A. M. Basahel, W. Ahmad and M. H. Sheikh, *Pet. Sci. Technol.*, 2015, **33**, 1190–1197.
58 C. Hogue, *Chem. Eng. News*, 2007.
59 T. Yang, L. Muzangwa, D. S. N. Parker, R. I. Kaiser and A. M. Mebel, *Phys. Chem. Chem. Phys.*, 2015, **17**, 530–540.
60 S. V. Levchik and E. D. Weil, *Polym. Adv. Technol.*, 2004, **15**, 691–700.
61 J. Huang, H. Meng, X. Luo, X. Mu, W. Xu, L. Jin and B. Lai, *Chemosphere*, 2021, 133112.
62 A. Zhang, Q. Ma, K. Wang, Y. Tang and W. A. Goddard, *USDOE Tech. Rep.*, 2005, 1–96.
63 A. Comandini, T. Malewicki and K. Brezinsky, *J. Phys. Chem. A*, 2012, **116**, 2409–2434.
64 R. Thilakaratne, J. Tessonnier and R. C. Brown, *Green Chem.*, 2016, **18**, 2231–2239.
65 X. Zhang and H. Lei, *RSC Adv.*, 2016, **6**, 6154–6163.
66 J. Aguado, D. P. Serrano, J. L. Sotelo, R. Van Grieken and J. M. Escola, *Ind. Eng. Chem. Res.*, 2001, **40**, 5696–5704.
67 S. Matsuura, T. Hashimoto and A. Ishihara, *Fuel Process. Technol.*, 2022, **227**, 107106.
68 C. Wang, H. Lei, M. Qian, E. Huo, Y. Zhao, Q. Zhang, W. Mateo, X. Lin, X. Kong, R. Zou and R. Ruan, *Sustain. Energy Fuels*, 2020, **4**, 4614–4624.
69 J. H. Harrhy, A. Wang, J. S. Jarvis, P. He, S. Meng, M. Yung, L. Liu and H. Song, *Commun. Chem.*, 2019, **2**, 1–13.
70 S. L. Wong, N. Ngadi, T. A. T. Abdullah and I. M. Inuwa, *Fuel*, 2017, **192**, 71–82.
71 Z. J. Buras, T. C. Chu, A. Jamal, N. W. Yee, J. E. Middaugh and W. H. Green, *Phys. Chem. Chem. Phys.*, 2018, **20**, 13191–13214.